NIH Public Access
Author Manuscript
Environ Sci Technol. Author manuscript; available in PMC 2012 September 1.

Published in final edited form as:
Environ Sci Technol. 2011 September 1; 45(17): 7345–7353. doi:10.1021/es201539s.

Kinetics and Mechanisms of Nanosilver Oxysulfidation

Jingyu Liu[1], **Kelly G. Pennell**[2], and **Robert H. Hurt**[3,4,*]

[1]Department of Chemistry, Brown University, Providence, Rhode Island 02912, USA

[2]Civil and Environmental Engineering Department, University of Massachusetts-Dartmouth, Dartmouth, Massachusetts 02747, USA

[3]School of Engineering, Brown University, Providence, Rhode Island 02912, USA

[4]Institute for Molecular and Nanoscale Innovation, Brown University, Providence, Rhode Island 02912, USA

Abstract

Among the many new engineered nanomaterials, nanosilver is one of the highest priority cases for environmental risk assessment. Recent analysis of field samples from water treatment facilities suggests that silver is converted to silver sulfide, whose very low solubility may limit the bioavailability and adverse impact of silver in the environment. The present study demonstrates that silver nanoparticles react with dissolved sulfide species (HS^-, S^{2-}) under relevant but controlled laboratory conditions to produce silver sulfide nanostructures similar to those observed in the field. The reaction is tracked by time-resolved sulfide depletion measurements to yield quantitative reaction rates and stoichiometries. The reaction requires dissolved oxygen, and it is sensitive to pH and natural organic matter. Focusedion-beam analysis of surface films reveals an irregular coarse-grained sulfide phase that allows deep (> 1 μm) conversion of silver surfaces without passivation. At high sulfide concentrations, nanosilver oxysulfidation occurs by a direct particle-fluid reaction. At low sulfide concentration, quantitative kinetic analysis suggests a mechanistic switch to an oxidative dissolution/precipitation mechanism, in which the biologically active Ag^+ ion is generated as an intermediate. The environmental transformation pathways for nanosilver will vary depending on the media-specific competing rates of oxidative dissolution and direct oxysulfidation.

Introduction

The broad use of silver nanoparticles (AgNPs) in consumer and medical products (1,2) coupled with the known ecotoxicity of some silver forms at low concentrations (3–5) make AgNPs one of the highest priority nanomaterials for environmental risk assessment (6). AgNPs-containing products may release silver to the environment in the form of ions, particles, or aggregates (7), and each of these forms can undergo further transformation in the environment in ways that affect silver fate, transport, and/or toxicity (1,8–10). One important transformation for AgNPs is particle-to-ion conversion, or dissolution, which can occur during use, product washing, or in the environment. Dissolution has been reported to

*Corresponding author phone: 401-863-2685; Fax: 401-863-9120; Robert_Hurt@brown.edu.

Supporting Information Available Detailed procedure for synthesizing citrate-stabilized AgNPs, TEM and DLS characterization of silver materials, soluble silver and sulfide measurements into $AgNO_3$-Na_2S mixtures, DO measurement at elevated sulfide and AgNP concentrations, oxidized sulfur species analysis during AgNP sulfidaton, effect of pH on AgNP sulfidation, UV-vis spectra recorded during AgNP sulfidation process, HRTEM images of sulfidated AgNPs, effect of NOM on AgNP sulfidation, and sulfur measurements into AgNPs-Na_2SO_4 and AgNPs-$Na2SO_3$ systems. This material is available free of charge via the Internet at http://pubs.acs.org.

NIH-PA Author Manuscript
NIH-PA Author Manuscript
NIH-PA Author Manuscript

NIH-PA Author Manuscript

NIH-PA Author Manuscript

NIH-PA Author Manuscript

be a heterogeneous oxidation reaction involving dissolved dioxygen and protons (8,11), and is influenced by natural organic matter (8), ligands (12), coatings (11,12), and pre-existing silver oxide or sulfide surface films (12). Both thermodynamic calculations and experimental data suggest that oxidized, not elemental silver will be the long-term preferred chemical form of silver in environmental compartments containing dissolved oxygen (8,12).

Recently, silver sulfide nanoparticles have been detected in the products of municipal and pilot-scale wastewater treatment plants (13,14), suggesting sulfidation as a second important environmental transformation. Silver sulfide, Ag_2S, in its low-temperature form acanthite (15) is highly insoluble (16) ($K = 6\times10^{-30}$ for the dissolution process: $Ag_2S + 2H^+ \leftrightarrow 2Ag^+ + H_2S(aq)$) so its formation can severely limit the concentration of soluble silver and the overall bioavailability and toxicity of environmental silver to aquatic organisms (1,5,17–19). The detection of silver sulfide nanoparticles in the field is an important finding, and we now need to understand more about their formation, behavior, and toxicity to fully understand the implications for environmental risk.

Silver sulfide, Ag_2S, is a form of oxidized silver, Ag(I), and there are two logical possibilities for its environmental formation mechanism. Silver sulfide nanoparticles, Ag_2S-NPs, may form by oxidative dissolution of AgNP followed by sulfide precipitation, or by direct conversion of AgNPs to Ag_2S-NPs through solid-fluid reaction. The distinction is important because the oxidative/precipitation (indirect) route produces an intermediate species of potentially high bioavailability and toxicity, Ag^+, where the direct route circumvents this biologically active species. Also, the precipitation pathway can occur for ionic releases associated with conventional silver sources unrelated to nanotechnology, which in recent estimates contributes significantly greater than AgNP to the total silver emission in the environment (20). It is an open question whether the Ag_2S-NPs observed in field studies are transformed AgNPs, or newly formed particles that precipitate when conventional soluble Ag releases contact environmental sulfide (13).

The nanoscience literature provides some information on formation routes for Ag_2S-NPs or related silver sulfide nanostructures. Pan et al. (21) synthesized water dispersible Ag_2S nanoparticles through aqueous chemical reaction of $AgNO_3$ with Na_2S in presence of capping agents. Kulkarni et al. (22) converted silver thin films to sulfidic thin films in aqueous Na_2S, and Chen et al. (23) assembled two-dimensional silver sulfide nanostuctures by reacting AgNP templates with H_2S in the gas phase. However, there is relatively little data relevant to environmental conversion. One recent study did focus on environmental transformation, and used TEM and X-ray techniques to characterize the solid phases formed by interaction of AgNPs with sulfide (24). The AgNPs are shown to convert to amorphous and crystalline sulfide phases in a manner that affects particle morphology, surface charge, and Ag^+ release rates (24).

The primary goal of the present study is to determine if the formation of silver sulfide nanoparticles reported recently (13,14) can be reproduced under controlled laboratory conditions to create similar solid-phase morphologies, and whether the reaction pathways proceeds primarily through the direct or indirect route. Additional important questions are the origin of superstoichiometric sulfides $Ag_2S_{n>1}$ reported in Kim et al. (13), and also the role of oxygen in the direct conversion route. The global reaction $2Ag^0 + S^{2-} \rightarrow Ag_2S$ is not charge balanced without an oxidant, and while O_2 (aq) is the most likely oxidant, sulfide concentrations are highest in anaerobic compartments in the environment, so the role of O_2 (aq) and its interplay with S^{2-} (aq) in the sulfidation process requires clarification. Finally it is unclear if the direct route can convert AgNPs fully to Ag_2S, or produce $Ag@Ag_2S$ core-shell structures, in which the early sulfide coating blocks access to the reactive core. The present study seeks answer each of these questions through controlled sulfidation

NIH-PA Author Manuscript

NIH-PA Author Manuscript

NIH-PA Author Manuscript

experiments on AgNPs in environmentally relevant, but well-defined fluid phases. We use time-resolved sulfide concentration measurement to monitor the sulfidation processes and a variety of materials diagnostic tools to characterize the solid-phase products. The effects of Ag dosage and size, dissolved oxygen, pH, and natural organic matter are investigated, and the data are used to construct AgNP sulfidation model under environmental relevant conditions.

Materials and Methods

Materials

Citrate-stabilized colloidal AgNPs (AgNPs-5 nm) were synthesized by a modified borohydride reduction procedure (8) (See the Supporting Information (SI)). Silver nanopowder (AgNPs-30 nm, average diameter 20–40 nm) manufactured by a vapor condensation process (QuantumSphere, CA, USA) was selected as low-functionalized commercial AgNP. Silver foil (99.9% Ag, 0.127mm thickness) and micron-sized silver powder (Ag-μm, 99.9% Ag, 1–3 μm) were used as additional reference materials (Strem Chemicals, MA, USA). The morphology and size distribution of silver materials were characterized by transmission electron microscope (TEM) and dynamic light scattering (DLS, Zetasizer Nano ZS system, Malvern Instruments), and are given in Figure S1 of SI. Silver concentrations were measured by graphite furnace atomic absorption (AA) spectrometry (PerkinElmer AAnalyst 600 GFAAs) after HNO_3 digestion (for total Ag) or after centrifugal ultrafiltration (for soluble Ag). Control experiment using $AgNO_3$ solution shows that the loss of Ag^+ (~15%) during ultrafiltration (Amicon Ultra-4 3K centrifugal tube, 30 min at 4000 g) is proportional to the input $AgNO_3$ concentration, which was used to derive soluble silver concentration from measured values.

Silver Sulfidation Experiments

The sulfidation process was monitored by measuring time-resolved depletion of soluble sulfide using a sulfide ion selective electrode (sulfide-ISE) following nanoparticle removal by centrifugal ultrafiltration. In a typical experiment, 4.9 mL DI water was added into a 15 mL plastic tube containing desired amount of AgNP-30 nm powder (0.324 – 5.393 mg), followed with sonication in a bath sonicator for 10 min to disperse aggregates, then 0.1 mL of 50 mM Na_2S solution was added to initiate the sulfidation reaction at a starting Na_2S concentration of 1 mM. The 1 mM Na_2S solution in DI water has an initial pH of 11.1 (Orion 8165BNWP pH electrode, Thermo Scientific), and the predominant sulfide species is HS^- (>99.9%) as calculated by visual MINTEQ (version 3.0). The reaction mixture was rotated at 20 rpm for up to 48 hrs, after which the sulfide-containing solution was separated from the solids using centrifugal ultrafiltration (Amicon Ultra-4 3K, cellulose membrane with 1–2 nm pore size, Millipore), at an relative centrifugal force of 4000 g for 25 min (Allegra X-15R, Beckman Coulter, Inc.). Then, a sulfide antioxidant buffer (SAOB, Orion 941609 Thermo Scientific) was added in equal volume to the collected sulfide-containing filtrate to prevent sulfide oxidation and volatilization during analysis. Soluble sulfide concentrations were measured with a sulfide-ISE (9616BNWP silver/sulfide combination electrode, Thermo Scientific) at room temperature, based on linear calibration curves constructed daily from fresh Na_2S standards in SAOB with detection limit of 6.25×10^{-3} mM. Any interference of silver ion with the sulfide-ISE was prevented by solution pretreatment with EDTA as the manufacturer recommends. This was confirmed by a special control experiment in which sulfide was measured in the presence of excess $AgNO_3$ (Figure S2).

The sulfidation stoichiometry was determined by measuring soluble sulfide depletion over 5-hr for a range of AgNP-30 nm concentrations (0.2 – 10 mM on Ag-atom basis, equivalent

NIH-PA Author Manuscript

NIH-PA Author Manuscript

NIH-PA Author Manuscript

to 21.6 – 1079mg/L) and selected sulfidation experiments were carried out under Ar purge to investigate the role of oxygen. Two silver samples with different particle size of 5 nm and 1~3 μm were also used to study surface area dependence. Selected experiments were conducted in media including humic acids (Suwannee River humic acid II standards, International Humic Substances Society) of 20 mg/L, at lower sulfide (0.1 and 0.25 mM), and at lower pH (50 mM pH7 phosphate buffer). All sulfidation experiments were conducted at room temperature and protected from room light.

The role of oxygen was investigated by carrying out sulfidation experiments under Ar purge (99.9% purity) using macroscopic silver foils (4 mm×4 mm×0.127 mm) followed by solid product characterization. In addition, dissolved oxygen (DO) levels were monitored in-situ during batch silver sulfidation experiments in a closed amber glass bottle under magnetic stirring using a DO probe (Orion 083010MD, Thermo Scientific) at 60 sec sampling frequency.

Solid Phase Characterization

The sizes and morphologies of pristine and sulfidated silver materials were characterized by TEM on a Philips CM20 at 200 kV, by high resolution TEM (HRTRM) on a JEOL 2010-HRTEM at 200 KV, and by scanning electron microscope (SEM) using a LEO 1530 field-emission SEM at low acceleration voltage (3–5 kV). To prepare TEM and SEM samples, a drop of silver-ethanol suspension (AgNPs-30 nm and Ag-μm) prepared using ultrasonication (Bransonic® 5510, Branson) or a drop of AgNPs-5 nm aqueous colloid was placed on a carbon coated copper TEM grid or on a silicon SEM substrate, followed by solvent evaporation at room temperature overnight. The surface sulfide layer thickness and morphology on silver foil reference samples were characterized by trench milling using a gallium focused ion beam (FIB) and viewed in cross-sections in situ by SEM, using a DualBeam FIB/SEM system (FEI Helios NanoLab600). The composition and phase of AgNP sulfidation products were identified by X-ray powder diffraction (XRD) spectrometry on a Bruker AXS D8-Advanced diffractometer with Cu *K*α radiation (λ = 1.5418 Å). To prepare the XRD samples, AgNP-30 nm powder (0.1 g) was sulfidated in Na_2S solution (200 mM, 5mL) overnight, followed by removal of chemical residues with repeated DI water wash, and blown with Ar overnight to obtain dry sulfidated powder.

Results

Sulfidation Pathways

Our early experiments showed a gradual decrease in sulfide concentration upon addition of silver nanoparticles, and a very rapid drop upon addition of soluble silver salts. These results along with previous observations of oxidative corrosion and Ag^+ release (8) lead to the scheme shown in Fig. 1, which illustrates competing reaction pathways for the sulfidation of AgNPs released to the environment. Additional experiments were designed to measure the time scales for sulfidation and the relative rates of the direct and indirect routes. Because the reaction between soluble sulfide and Ag^+ is very rapid, the second step in the indirect route will not typically be rate limiting. The experiments therefore focus on the rate of direct sulfidation and its comparison to previously measured rates of oxidative dissolution (8,12), which is the rate-limiting step in the indirect route.

Reaction Rates and Stoichiometries

To determine quantitative rates and stoichiometries, a method was developed to track the progress of silver sulfidation by time-resolved measurement of free sulfide depletion. At defined times, the residual sulfide ($H_2S_{(aq)}/HS^-S^{2-}$) in Na_2S solutions containing AgNPs was measured using sulfide-ISE following nanoparticle removal by centrifugal

NIH-PA Author Manuscript

NIH-PA Author Manuscript

NIH-PA Author Manuscript

ultrafiltration. Figure 2A clearly shows a particle-sulfide reaction (lower curve) that is much faster than solution-phase sulfide oxidation (upper curve). Figure 2B shows data at longer times and for a range of AgNP concentrations. Here the slow loss of sulfide is seen in the particle-free solution, presumably by homogeneous oxidation, and the particle-mediated reactions are rapid and have a two-stage nature. The first stage is fast and transitions at about 5 hrs to a slower reaction through a distinct elbow in each curve. Figure 2C focuses on the first reaction stage and shows that total sulfide consumption after 5 hrs is approximately 1/2 the AgNP concentration on a molar basis (dashed line) suggesting Ag_2S as the primary first-stage reaction product. Support for this stoichiometry is given in the XRD spectra of Fig. 3A, which shows FCC zero-valent AgNP conversion to Ag_2S acanthite phase after overnight reaction with Na_2S. It should be noted that the amount of Ag_2S in the AgNP sulfidation product may be underestimated by XRD due to the formation of amorphous Ag_2S phases (24). During the reaction we observed colloidal destabilization and settling of suspended AgNP powders, and TEM (Fig. 3B and 3C) confirm the formation of micrometer scale aggregates, suggesting sulfidation not only transforms the AgNP chemistry, but will likely also influence particle fate and transport by altering colloidal dynamics.

These sulfidation reaction times (~5 hrs) are much shorter than previously reported times for AgNP oxidative dissolution, where a surface recession rate of order 0.7 nm/day in air-saturated water at neutral pH gives 4 – 43 day dissolution periods depending on particle size (8,12). Similar sulfidation is observed at lower sulfide concentration (0.1 mM and 0.25 mM, data not shown). This indicates the sulfidation must be direct (Fig. 1) and not the result of dissolution/precipitation under these laboratory conditions where sulfide concentrations are much elevated (0.32–32 mg/L) relative to those in the natural environment (25–28).

Reaction Mechanism – Oxysulfidation

The reaction $2Ag + S^{2-} \rightarrow Ag_2S$ is charge unbalanced without an oxidant, which in this simple reaction medium is likely to be dissolved oxygen (DO). We first designed a simple "tarnishing" experiment to investigate the role of DO. Silver foils were immersed overnight in either air-saturated or Ar-purged Na_2S solutions, and their surfaces imaged under visible light. In aerobic conditions a dark gray sulfidic scale forms, possibly Ag_2S (29) (Fig. 4A). The effect of DO removal by Ar purge is striking – Fig. 4A shows the complete suppression of the visible sulfidic film, confirming the need for O_2 to remove electrons and charge balance the silver sulfidation process. The role of DO is also clearly seen in the free sulfide measurements in Fig. 4B, which only respond to AgNPs if oxygen is present, and in direct measurements of DO (Fig. 4C), which decrease in a closed container in the presence of sulfide and AgNPs. We also observed the DO depletion was greatly accelerated at elevated Na_2S and AgNP concentrations (SI, Fig. S3).

These results confirm that the primarily reaction is an oxysulfidation, which at near-neutral pH can be written as a combination of

$$4Ag + O_2 + 2H_2S \rightarrow 2Ag_2S + 2H_2O \quad \text{(Eq. 1a)}$$

$$4Ag + O_2 + 2HS^- \rightarrow 2Ag_2S + 2OH^- \quad \text{(Eq. 1b)}$$

AgNP Oxysulfidation Kinetics

The rate data in Fig. 2B is suitable for limited quantitative kinetic analysis. When sulfide is in excess ([S] > ½ [Ag]), the Fig. 2B data exhibit a two-stage (fast/slow) behavior. The initial, fast stage (0–5 hr) is consistent with Ag_2S formation as discussed above, while the

NIH-PA Author Manuscript

NIH-PA Author Manuscript

NIH-PA Author Manuscript

second, slow stage represents either the formation of superstoichiometric sulfides, $Ag_2S_{n>1}$ (13), and/or particle catalyzed sulfide oxidation (30) (SI, Fig. S4). Figure 5A shows a log-linear relationship between sulfide concentration and time in the initial fast sulfidation stage, $\ln[\text{sulfide}]/[\text{sulfide}]_0 = -k_{obs}\times t$, suggesting a rate law: $-d[\text{sulfide}]/dt = k_{obs}\times[\text{sulfide}]$, and Fig. 5B shows k_{obs} to be proportional to [AgNP] as expected for a heterogeneous reaction process. Overall we propose the following kinetic law for the primary sulfidation:

$$-(d[\text{sulfide}])/dt = \left(k_a \bullet [\text{AgNP}]_{\text{initial}} + k_{homogen}\right) \times [\text{sulfide}]^n \quad \text{(Eq. 2)}$$

where n=1. Fitting Fig. 2B data yields: k_a = 0.0051 ($mM^{-1}\bullet min^{-1}$) and $k_{homogen}$ = 0.00016 (min^{-1}) in simple media with pH near 11. The dashed lines in Fig. 2B show the overall fit of this model and parameter set. This reaction is faster at lower pH and gives a k_a at pH 7 (SI, Fig. S5) of:

$$k_a = 0.018\left(mM^{-1} \bullet min^{-1}\right) \quad \text{(Eq. 3)}$$

which is recommended for modeling purposes, and is specific to 30 nm particles in simple media.

Fig. 6 shows the effect of Ag particle size from 5 nm to 2 μm at constant silver/sulfide ratio. Increasing particle size reduces reaction rates as expected for the direct process that depends on specific surface area. Interestingly, the reaction eventually runs to completion even for the largest particles (2 μm), indicating that sulfidation does not produce uniform films that protect a zero-valent core. To better understand how large particles are fully converted to sulfides, we sulfidated macroscopic silver films and studied the morphology of the reaction products using SEM on cross-sections produced by focused gallium ion beam. Figure 6B shows that the sulfidic films are not similar to the original silver surface, but consist of irregular micron-scale grains that appear to have crystallized and protruded from the substrate surface. The cross-sectional view gives a typical product film height of 3–4 μm. For comparison, Kulkarni et al.(22) reported formation of a 300 nm Ag_2S film by dipping a silver film in Na_2S for 10min. The observed structure of large, micron-scale irregular grains suggests why sulfide coatings do not protect unreacted metallic cores from further sulfidation in fine particles, at least under these conditions. HRTEM image (Fig. 6C) of sulfidated 5 nm AgNPs further confirms the complete conversion of silver phase to Ag_2S phase. Interestingly, we observed a color change during sulfidation of this colloidally stable AgNP sample, indicating a shift in the surface plasmon resonance wavelength, which was confirmed by UV-vis spectrometry (SI, Fig. S6). And HRTEM images show that AgNPs coalesce and form a network structure during sulfidation (SI, Fig. S7), which is further confirmed by size distribution measurement of AgNPs-5 nm during sulfidation (Fig. 6D).

Effects of NOM and pH

Figure 7 shows the dependence of sulfidation rate on natural organic matter. Organic matter in natural waters mediate many nanoparticle processes, including stability (31), dissolution (8) and aggregation (10). Figure 7A shows that humic acid slightly increases sulfidation rates, and enhanced sulfide depletion was also observed in particle free humic acid solution (SI, Fig. S8). However sulfide-NOM reaction alone cannot compensate the effect of NOM in Fig. 7A, the improvement in colloidal stability may be responsible for the role of NOM played in AgNP sulfidation. Environmental sulfides are primarily in the form of $HS^-$and H_2S, and speciation may influence AgNP sulfidation. The above experiments were carried out in DI water with initial [Na_2S] at 1mM, where solution pH was 11.1 and HS^- was the

NIH-PA Author Manuscript

NIH-PA Author Manuscript

NIH-PA Author Manuscript

predominant sulfide species (>99.9%). Experiments in phosphate buffers (pH 7) show that reduced pH increases reaction rates (SI, Fig. S5).

Discussion

Though silver is a noble metal, nanosilver is far from chemically inert in the environment. It undergoes oxidation and ion release that can lead to complete dissolution (8,12), and recent field studies suggest it can also undergo near-complete sulfidation (13,14). The present laboratory study demonstrates that AgNPs can react with dissolved sulfide species ($H_2S_{(aq)}$, HS^-) to produce silver sulfide nanostructures similar to those observed in field samples confirming the basic feasibility of direct particle-to-particle conversion. The data in Figures 2–7 reveal some basic features of this reaction: it is an oxysulfidation entirely dependent on the presence of at least some dissolved dioxygen; it is influenced by particle size and NOM; and is approximately first-order in sulfide over the limited range studied. The requirement for both DO and sulfide raises an interesting question about the physical location of this transformation in the environment. Sulfur in aerobic environments exists primarily as sulfate, and we observe no reaction between AgNPs and sulfate, or sulfite (SI, Fig. S9). Sulfide in oxic waters can be at ppt levels (25,26), which may lead to very low rates of silver sulfidation. High sulfide levels are usually associated with anaerobic conditions, but if oxygen is completely absent, our results suggest that sulfidation will be suppressed. It is likely that nanosilver oxysulfidation occurs preferentially in anaerobic environments, such as the first mixing tank as reported in the Kaegi et al. study (14), where sulfide concentrations are elevated, but there is residual oxygen. Dissolved oxygen and sulfide do not coexist at equilibrium but can coexist in non-equilibrium mixing zones. In the submerged portions of sewer lines, for example, anaerobic biofilms can engage in sulfate respiration to produce sulfide, which can be transported into adjacent oxygen containing regions (32).

In the present study we observe direct AgNP conversion to sulfidic particles (direct route in Fig. 1). The indirect route cannot be responsible for the main AgNP conversion seen here, because its first step (oxidative ion release) has been extensively characterized (8) and is orders of magnitude slower than the observed sulfidation, and a series reaction cannot be faster than one of its constituent steps. We note, however, that in cases where preoxidation gives rise to silver oxide films, silver chloride films, or an inventory of Ag^+ complexed on polymer coatings, this soluble silver fraction can release quickly and react with sulfide homogeneously to form distinct Ag_2S particles, surface precipitates, or bridges by the indirect route. In the present case and in many cases, the majority of silver in AgNPs is zero valent and must be oxidized by the slow chemical reaction with O_2 and H^+, and this step makes the indirect route too slow to compete with the direct route we observe here. This observed preference for the direct route, however, is a consequence of the high sulfide concentrations chosen to achieve convenient reaction times in the laboratory. The sulfide concentrations used here (3.2 – 32 mg/L) are at the upper end of those relevant to environment, which extend downward over many orders of magnitude, leaving open the question of the mechanism in low-sulfide waters. Figure 8 explores the relations between sulfidation rates, reactive dissolution rates, and residence times over a much wider range of conditions. This model calculation is based on 30 nm silver particles, the sulfidation kinetic law in Eq. 2 with the neutral-pH rate constant in Eq. 3, and a typical oxidative dissolution rate near neutral pH that gives an 15-day half-life in air-saturated water (8,12). The Figure compares the time scales for direct sulfidation (particle-to-particle conversion, red line) and indirect sulfidation (oxidative dissolution and sulfide precipitation, black horizontal line). Under our elevated sulfide conditions in the laboratory, and under many conditions in sewer lines and water treatment facilities, the direct sulfidation times are shorter than dissolution times, and direct particle-to-particle conversion is expected. At lower sulfide, this

NIH-PA Author Manuscript

NIH-PA Author Manuscript

NIH-PA Author Manuscript

calculation predicts a mechanistic switch to the indirect conversion, which generates the active Ag^+ species as an intermediate.

The probability that nanosilver will undergo sulfidation before reaching sensitive environmental receptors can be seen by comparing the residence times (shaded boxes) with the shorter of the two times that describe the parallel reaction routes. Under our laboratory conditions, and under some conditions in sewer lines and water treatment facilities, there is sufficient time for complete or near-complete sulfidation, consistent with the recent field reports (13,14). If conversion is incomplete, or if these treatment systems are bypassed, nanosilver will reach low-sulfide waters and Figure 8 predicts it will preferentially undergo slow oxidative dissolution. Water treatment facilities may be bypassed during overflow conditions, or when nanosilver is released outdoors, following landfill disposal of nanosilver products, or the use of outdoor nanosilver products such as sailcloth, tarps, tents, or awnings. The direct release of AgNPs to low-sulfide oxic waters can be expected to produce Ag^+ as an intermediate state, which increases the potential for uptake, bioaccumulation and adverse biological or ecological implications. Also, since oxidative dissolution is a slow process, it is likely that AgNPs themselves could reach sensitive receptors followed by uptake, internalization, and dissolution.

Environmental oxysulfidation reactions appear to be important behaviors that mediate nanosilver environmental risks. More work is needed in this area, in particular on the behavior at very low sulfide concentrations and in presence of other potential environmental oxidants, the behavior in complex field samples, and on the fate, transport, and toxicity of the Ag_2S_n reaction products, which are likely candidates for the end state of the element silver released to the natural environment.

Supplementary Material

Refer to Web version on PubMed Central for supplementary material.

Acknowledgments

Financial support was provided by NSF grant ECCS-1057547, EPA STAR grant R833862, and the Superfund Research Program of the National Institute of Environmental Health Sciences, P42ES013660. Although sponsored in part by the EPA and NIEHS, this work does not necessarily reflect the views of either agency. The technical contributions of David Murray, Joseph Orchardo and Anthony McCormick at Brown University are gratefully acknowledged.

Literature Cited

(1). Nowack B. Nanosilver revisited downstream. Science. 2010; 330(6007):1054–1055. [PubMed: 21097924]

(2). Chaloupka K, Malam Y, Seifalian AM. Nanosilver as a new generation of nanoproduct in biomedical applications. Trends Biotechnol. 2010; 28(11):580–588. [PubMed: 20724010]

(3). Ratte HT. Bioaccumulation and toxicity of silver compounds: A review. Environ. Toxicol. Chem. 1999; 18(1):89–108.

(4). Shoults-Wilson WA, Zhurbich OI, McNear DH, Tsyusko OV, Bertsch PM, Unrine JM. Evidence for avoidance of Ag nanoparticles by earthworms (*Eisenia fetida*). Ecotoxicology. 2011; 20(2): 385–396. [PubMed: 21229389]

(5). Fabrega J, Luoma SN, Tyler CR, Galloway TS, Lead JR. Silver nanoparticles: behaviour and effects in the aquatic environment. Environ. Int. 2011; 37(2):517–531. [PubMed: 21159383]

(6). Stone V, Nowack B, Baun A, van den Brink N, van der Kammer F, Dusinska M, Handy R, Hankin S, Hassellöv M, Joner E, Fernandes TF. Nanomaterials for environmental studies: Classification, reference material issues, and strategies for physico-chemical characterization. Sci. Total Environ. 2010; 408(7):1745–1754. [PubMed: 19903569]

NIH-PA Author Manuscript

NIH-PA Author Manuscript

NIH-PA Author Manuscript

(7). Benn. TM, Westerhoff P. Nanoparticle silver released into water from commercially available sock fabrics. Environ. Sci. Technol. 2008; 42(11):4133–4139. [PubMed: 18589977]

(8). Liu J, Hurt RH. Ion release kinetics and particle persistence in aqueous nano-silver colloids. Environ. Sci. Technol. 2010; 44(6):2169–2175. [PubMed: 20175529]

(9). Akaighe N, MacCuspie RI, Navarro DA, Aga DS, Banerjee S, Sohn M, Sharma VK. Himic acid-induced silver nanoparticle formation under environmentally relevant conditions. Environ. Sci. Technol. 2011; 45(9):3895–3901. [PubMed: 21456573]

(10). Fabrega J, Fawcett SR, Renshaw JC, Lead JR. Silver nanoparticle impact on bacterial growth: effect of pH, concentration, and organic matter. Environ. Sci. Technol. 2009; 43(19):7285–7290. [PubMed: 19848135]

(11). Kittler S, Greulich C, Diendorf J, Köller M, Epple M. Toxicity of silver nanoparticle increases during storage because of slow dissolution under release of silver ions. Chem. Mater. 2010; 22(16):4548–4554.

(12). Liu J, Sonshine DA, Shervani S, Hurt RH. Controlled release of biologically active silver from nanosilver surfaces. ACS Nano. 2010; 4(11):6903–6913. [PubMed: 20968290]

(13). Kim B, Park C, Murayama M, Hochella MF Jr. Discovery and characterization of silver sulfide nanoparticles in final sewage sludge products. Environ. Sci. Technol. 2010; 44(19):7509–7514. [PubMed: 20839838]

(14). Kaegi R, Voegelin A, Sinnet B, Zuleeg S, Hagendorfer H, Burkhardt M, Siegrist H. Behavior of metallic silver nanoparticles in a pilot wastewater treatment plant. Environ. Sci. Technol. 2011; 45(9):3902–3908. [PubMed: 21466186]

(15). Bell RA, Kramer JR. Structural chemistry and geochemistry of silver-sulfur compounds: critical review. Environ. Toxicol. Chem. 1999; 18(1):9–22.

(16). Haynes, WM., editor. CRC Handbook of Chemistry and Physics. 91st Edition. CRC Press/Taylor and Francis; Boca Raton, FL: Solubility Product Constants. Internet Version 2011

(17). Choi O, Clevenger TE, Deng B, Surampalli RY, Ross L, Hu. Z. Role of sulfide and ligand strength in controlling nanosilver toxicity. Water Res. 2009; 43(7):1879–1886. [PubMed: 19249075]

(18). Hogstrand C, Wood CM. Toward a better understanding of the bioavailability, physiology, and toxicity of silver in fish: implications for water quality criteria. Environ. Toxicol. Chem. 1998; 17(4):547–561.

(19). Luoma, SN. Silver nanotechnologies and the environment: old problems or new challenges?. Woodrow Wilson International Center for Scholars; Washington, DC: 2008.

(20). Nowack B, Krug HF, Height M. 120 Years of Nanosilver History: Implications for policy makers. Environ. Sci. Technol. 2011; 45(4):1177–1183.

(21). Pan H, Tao X, Mao C, Zhu J, Liang F. Aminopolycarboxyl-modified Ag_2S nanoparticles: Synthesis, characterization and resonance light scarttering sensing for bovine serum albumin. Talanta. 2007; 71(1):276–281. [PubMed: 19071300]

(22). Kulkarni AB, Uplane MD, Lokhande CD. Preparation of silver sulphide from chemically deposited silver films. Mater. Chem. Phy. 1995; 41(1):75–78.

(23). Chen R, Nuhfer NT, Moussa L, Morris HR, Whitmore PM. Silver sulfide nanoparticle assembly obtained by reacting an assembled silver nanoparticle template with hydrogen sulfide gas. Nanotechnol. 2008; 19(45):455604–455615.

(24). Levard C, Reinsch BC, Michel M, Oumahi C, Lowry GV, Brown GE Jr. Sulfidation processes of PVP-coated silver nanoparticles in aqueous solution: Impact on dissolution rate. Environ. Sci. Technol. 2011; 45(12):5260–5266. [PubMed: 21598969]

(25). Luther GW, Tsamakis E. Concentration and form of dissolved sulfide in the oxic water column of the ocean. Marine Chem. 1989; 27(3–4):165–177.

(26). Tang D, Santschi PH. Sensitive determination of dissolved sulfide in estuarine water by solid-phase extraction and high-performance liquid chromatography of methylene blue. J. Chromatogr. A. 2000; 883(1–2):305–309. [PubMed: 10910224]

(27). Kuwabara JS, Luther GW. Dissolved sulfides in the oxic water column of San Francisco Bay, California. Estuaries. 1993; 16(3A):567–573.

NIH-PA Author Manuscript

NIH-PA Author Manuscript

NIH-PA Author Manuscript

(28). Cowan CE, Jenne EA, Crecelius EA. Silver speciation in seawater: the importance of sulfide and organic complexation. Marine and Estuarine Geochemistry. 1985:285–304.

(29). Saber TMH, EL Warraky AA. AES and XPS study on the tarnishing of silver in alkaline sulphide solutions. J. Mater. Sci. 1988; 23(4):1496–1501.

(30). Hoyer P, Weller H. Particle size and pH effects on the sensitization of nanoporous titanium dioxide electrodes by Q-sized silver sulfide. Chem. Phys. Lett. 1994; 224(1–2):75–80.

(31). Cumberland SA, Lead JR. Particle size distributions of silver nanoparticles at environmentally relevant conditions. J. Chromatogr. A. 2009; 1216(52):9099–9105. [PubMed: 19647834]

(32). Hvitved-Jacobsen, T. Sewer Processes: Microbial and Chemical Process Engineering of Sewer Networks. 1st, ed.. CRC Press; Boca Raton, FL: 2002.

(33). Shammas, NK.; Wang, LK. Fair, geyer and okun's water and wastewater engineering: Water supply and wastewater removal. 3rd, ed.. John Wiley & Sons; Hoboken, NJ: 2011.

(34). Davis, M. Water and Wastewater Engineering: Design Principles and Practice. McGraw-Hill Higher Edication; NY: 2011.

NIH-PA Author Manuscript

NIH-PA Author Manuscript

NIH-PA Author Manuscript

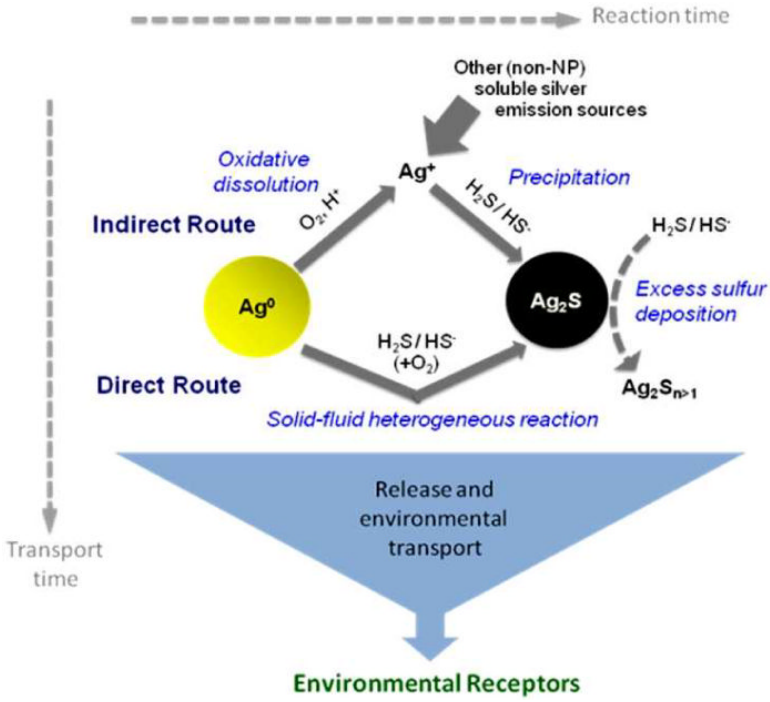

FIGURE 1.

Competing chemical and transport pathways of nanosilver sulfidation released to the environment. Ag_2S-NPs may be produced by particle-fluid reaction (direct route) or by oxidative dissolution to soluble silver followed by sulfide precipitation (indirect route). The main chemical pathway to Ag_2S will depend on the relative rates of these two reactions as a function of media compositions along the AgNP transport trajectory. Figure 1 also shows the possible role of oxygen in direct sulfidation, and the possible formation of superstoichiometric sulfide phases as reported by Kim (13). A competition between sulfidation reaction times (horizontal axis) and transport times (vertical axis) determines whether the biologically active Ag^+ and AgNP phases reach sensitive biological receptors before they are transformed into the more benign sulfide phases.

NIH-PA Author Manuscript

NIH-PA Author Manuscript

NIH-PA Author Manuscript

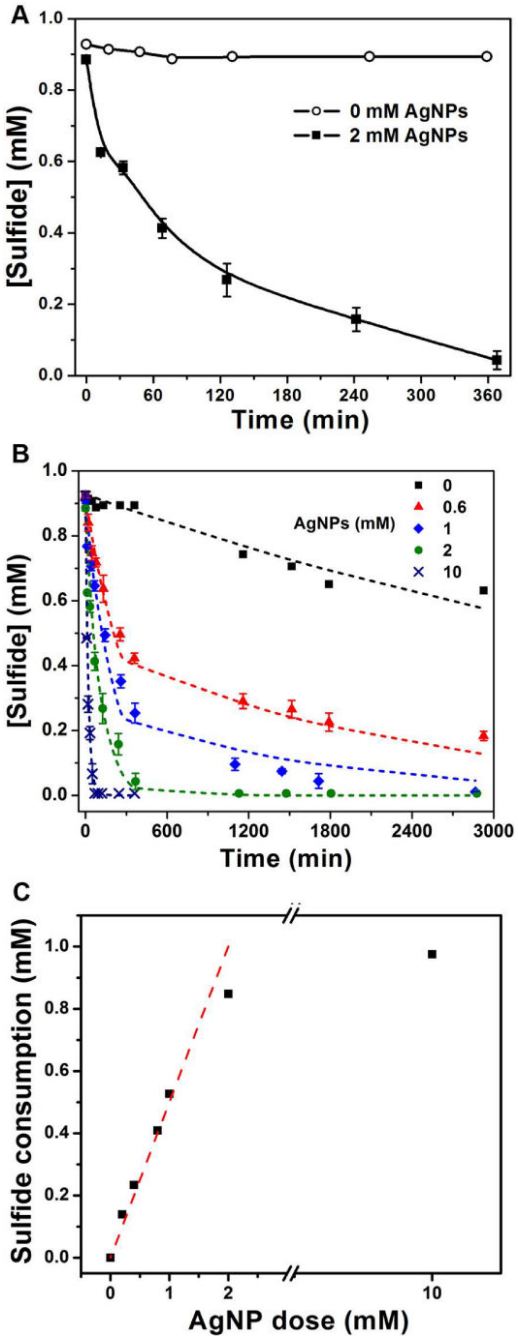

FIGURE 2.

Sulfide depletion rates due to AgNP-Na_2S reaction. (A) Time-resolved depletion of sulfide from 1 mM Na_2S solutions in presence of 2 mM AgNPs (Note: 2 mM is molar concentration of Ag atoms in the system, equivalent to 215.7 mg/L). Sulfide depletion in the particle-free solution is negligible. (B) Longer-time data showing slow homogeneous oxidation of sulfide and rapid two-stage reaction in the presence of AgNPs. Data show three independent replicates. (C) 5-hr consumption of sulfide (at stage 1/stage 2 transition) as function of AgNP loading, showing the stiochiometric relation: $\Delta[\text{sulfide}] = \frac{1}{2}[\text{Ag}]_{\text{input}}$ (dashed line) consistent with Ag_2S as main product.

NIH-PA Author Manuscript

NIH-PA Author Manuscript

NIH-PA Author Manuscript

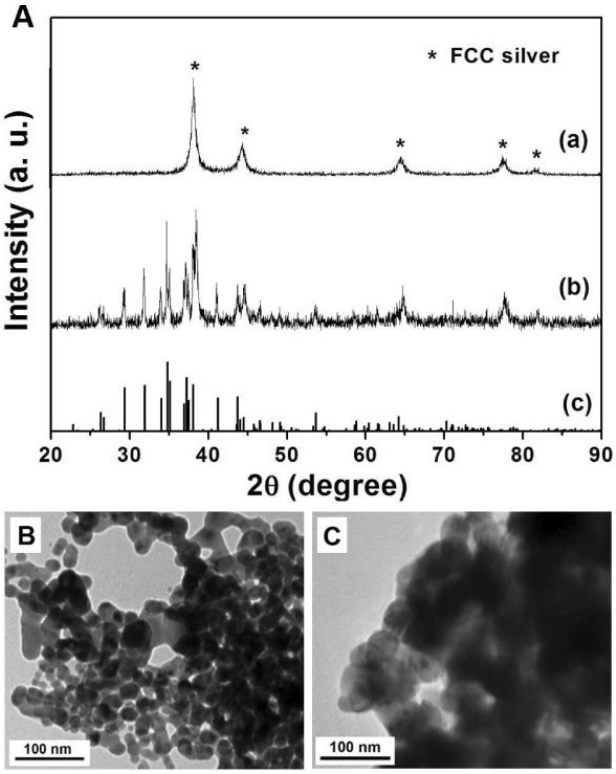

FIGURE 3.

Phase and morphology characterization of AgNP sulfidation products. (A) Identification of AgNP sulfidation products by XRD spectrometry: (a) pristine AgNP-30 nm powder, identified as FCC zero-valent metal; (b) Same AgNPs sulfidated in Na_2S overnight; (c) Ag_2S reference XRD pattern for acanthite, which appears to be a major phase in (b). (B) TEM image of pristine AgNP powder with particle diameter of 20–40 nm. (C) TEM image of sulfidated AgNPs.

NIH-PA Author Manuscript

NIH-PA Author Manuscript

NIH-PA Author Manuscript

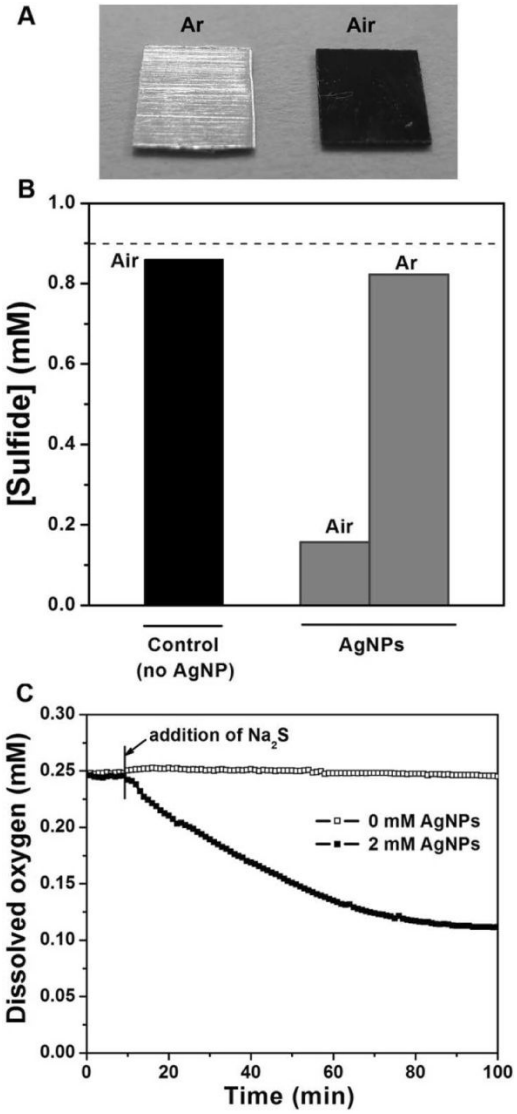

FIGURE 4.

Evidence for oxysulfidation as reaction mechanism. (A) Optical images of silver foil (99.9% Ag) incubated in air-saturated (right) and Ar-purged (left) Na_2S solutions (0.1 mM) at room temperature for 1 day, showing sulfidic scale only in the presence of dissolved oxygen. (B) Free sulfide also decreases in the presence of AgNPs and air (4-hr treatment), but not in the presence of AgNPs under Ar purge. The dashed line represents the initial Na_2S concentration (AgNP-30 nm powder were added at 2 mM on Ag-atom basis). (C) On-line DO measurements in 1mM Na_2S solution showing depletion only in the presence AgNP-30nm powder.

NIH-PA Author Manuscript

NIH-PA Author Manuscript

NIH-PA Author Manuscript

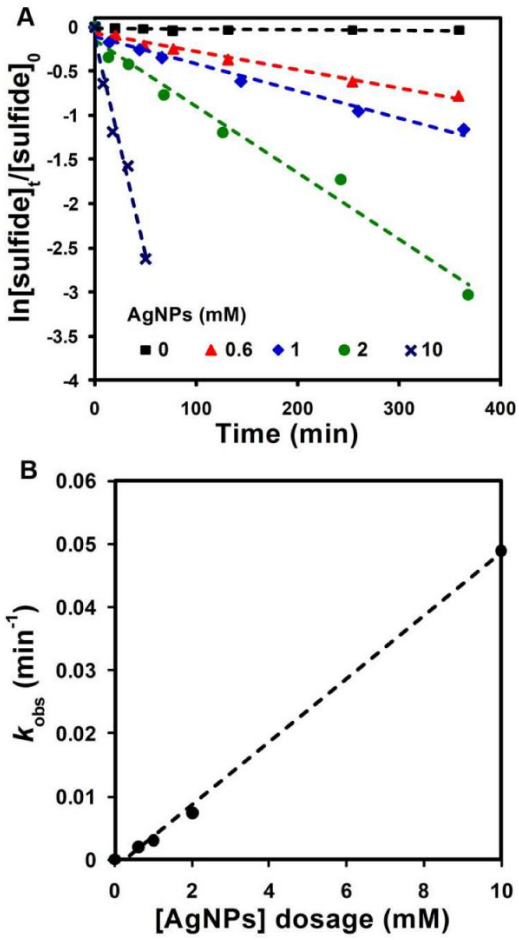

FIGURE 5.

AgNP oxysulfidation is a direct, heterogeneous reaction. (A) Log-linear relationship between sulfide concentration and time, suggesting a rate law: $-d[\text{sulfide}]/dt = k_{obs} \times [\text{sulfide}]$. Data show the average of three independent replicates. (B) The observed rate constants derived from (A) as function of AgNP concentration, showing linear correlation $k_{obs} = 0.0051\ (\text{mM}^{-1};\bullet\text{min}^{-1}) \times [\text{AgNP}]_{\text{input}}$ (mM on Ag-atom basis)

NIH-PA Author Manuscript

NIH-PA Author Manuscript

NIH-PA Author Manuscript

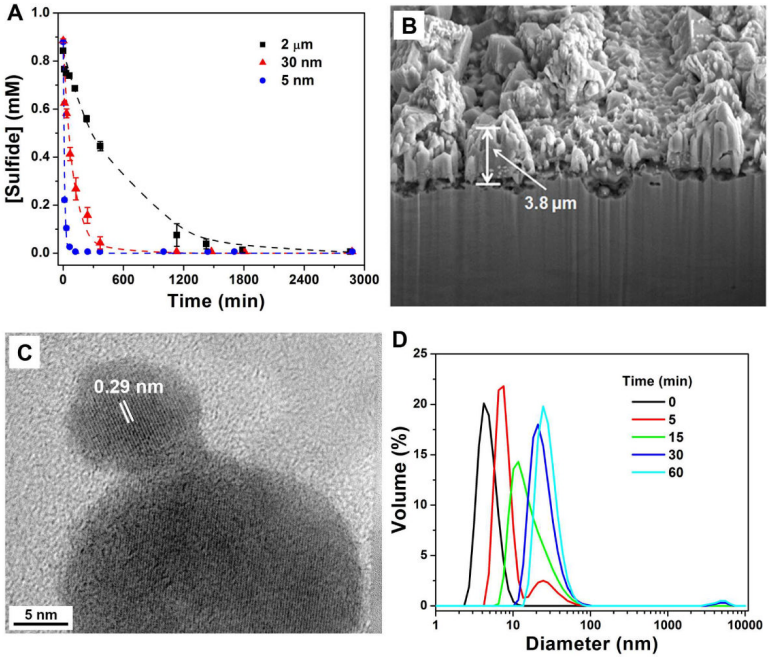

FIGURE 6.

Effect of particle size on silver sulfidation rates. (A) Time-resolved sulfide depletion as function of silver particles sizes ($[Ag]_{input}$=2 mM on Ag-atom basis). (B) SEM image of Ag_2S scale formed on silver foil surfaces. The FIB-etched cross-section shows a typical height of 3–4 μm for the Ag_2S grains. Sample was prepared by incubating a silver foil (4 mm×4 mm×0.127 mm) in Na_2S solution (1mM, 10 mL) at room temperature in ambient air for 1d. (C) HRTEM image of sulfidated 5 nm AgNPs (215.7 mg/L AgNPs in 1 mM Na_2S for 1 day), showing lattice fringes of 0.29 nm spacing, which is close to the (−112) plane spacing of Ag_2S. (D) DLS measured size distribution of AgNPs-5 nm during sulfidation, indicating particle aggregation ($[Ag]_{input}$=215.7 mg/L, $[Na_2S]_{input}$=1 mM).

NIH-PA Author Manuscript

NIH-PA Author Manuscript

NIH-PA Author Manuscript

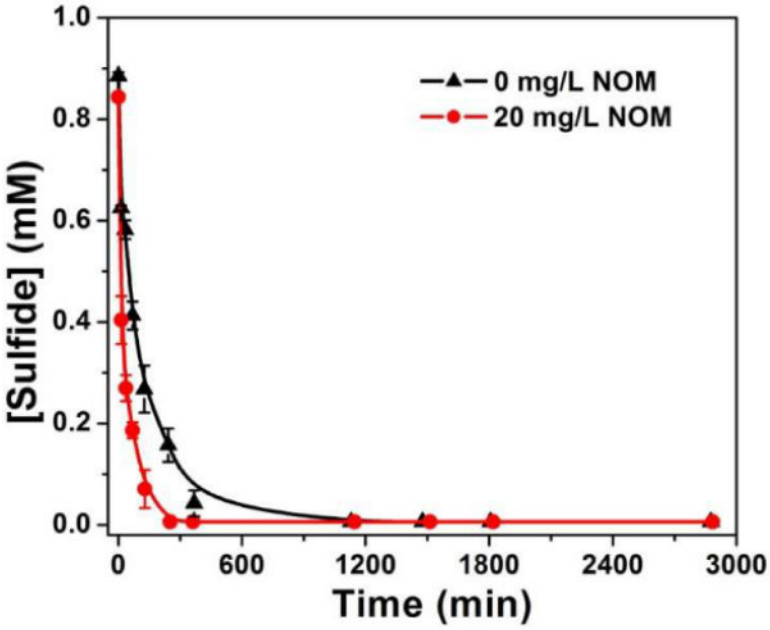

FIGURE 7.

Effect of natural organic matter on AgNP sulfidation. Time-resolved sulfide depletion measurements of AgNP powder-Na_2S reaction in DI water and NOM solutions. Suwannee river humic acid used at 20 mg/L ($[Ag]_{input}$ = 2 mM at Ag-atom basis).

NIH-PA Author Manuscript

NIH-PA Author Manuscript

NIH-PA Author Manuscript

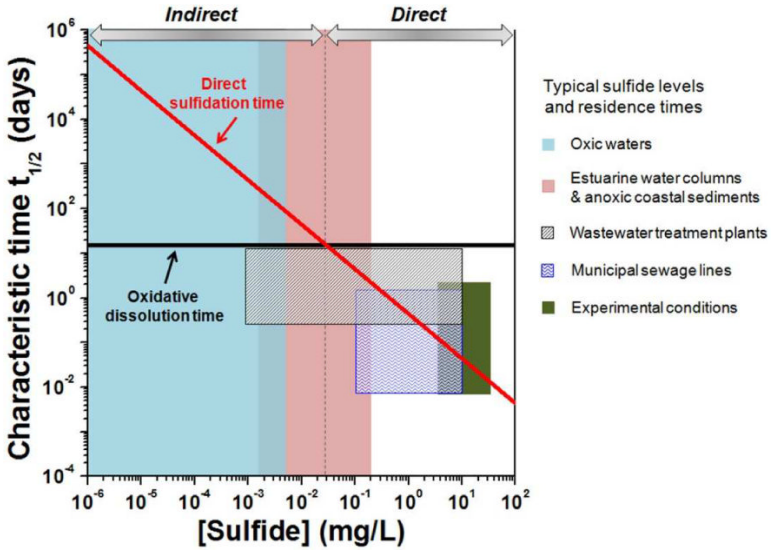

FIGURE 8.

Modeling of AgNP oxysulfidation over a wide range of sulfide concentration. The red line gives estimated reaction times for direct sulfidation route as a function of sulfide concentration, using the kinetics of Eq. 2, for 30 nm AgNPs in air-saturated environments. The black line gives the time scale for indirect route which is determined by the rate limiting step of AgNP oxidative dissolution and is independent to sulfide concentration. The crossing point, [sulfide] = 0.025 mg/L, is an estimate of the sulfide concentration at which there is a switch from direct to indirect sulfidation. The shaded squares give typical ranges for sulfide concentration and residence time in key compartments: fully oxic water columns – typically in ppt to ppb levels (25–27); estuarine water columns and above anoxic coastal sediments – 1.7 ~ > 100 ug/L (28); municiple sewage lines – 0.1 to 10 mg/L (32), 10 min to 1.5 day (33); WWTP – ppb to 10 mg/L, 6 hr (34) to 14 days. Note the maximum sulfide concentration in WWTP was based on upper concentration of influent water, and the time was selected by accounting for wastewater and sludge treatment. The model suggests that municipal sewer lines and water treatment plants may be able to transform AgNPs to sulfides, and the primary route will be direct solid-fluid reaction. In contrast, environmental releases reach natural waters, may lead to much slower sulfidation, and to a primary reaction mechanism that is indirect - passing through the soluble silver ion as a biologically active intermediate.